

Positioning with medium frequency R-Mode

Lars Grundhöfer¹  | Filippo Giacomo Rizzi¹ | Stefan Gewies¹  |
Michael Hoppe² | Jesper Bäckstedt³ | Marek Dziewicki⁴ | Giovanni Del Galdo^{5,6} 

¹ Institute of Communications and Navigation, German Aerospace Center, Neustrelitz, Germany

² German Federal Waterways and Shipping Administration, Koblenz, Germany

³ Swedish Maritime Administration, Norrköping, Sweden

⁴ Maritime Office Gdynia, Gdynia, Poland

⁵ Institute for Information Technology, Technische Universität Ilmenau, Ilmenau, Germany

⁶ Fraunhofer Institute for Integrated Circuits IIS, Ilmenau, Germany

Correspondence

Lars Grundhöfer, Institute of Communications and Navigation, German Aerospace Center, Neustrelitz, Germany.
Email: lars.grundhoefer@dlr.de

Present Address

German Aerospace Center, Kalkhorstweg 53, 17235 Neustrelitz, Germany

Funding information

European Regional Development Fund

Abstract

R-Mode is a terrestrial navigation system under development for the maritime domain that provides backup in case of a GNSS outage. This paper describes the first test results for real-time positioning on board a ship using medium frequency R-Mode signals. The estimation and positioning algorithms used are described in detail and it is shown how they are integrated into the R-Mode receiver developed by the German Aerospace Center. Moreover, during two day-time experiments with lower and higher dynamic movements of a ship in the Baltic Sea, we were able to achieve a 95% horizontal positioning accuracy of better than 12 m in the center of three R-Mode transmitters. This demonstrates the first time that the medium frequency R-Mode has provided positioning at sea.

KEYWORDS

backup, PNT, R-Mode, terrestrial navigation

1 | INTRODUCTION

Ranging Mode (R-Mode) is a maritime terrestrial navigation system that is currently under development (Gewies et al., 2018; Jiang et al., 2018; Johnson et al., 2020; Swaszek, 2014; Wirsing et al., 2020). It enables positioning and timing on the water up to distances of a few hundred kilometers from shore if a sufficient number of R-Mode signals are available (Koch & Gewies, 2020). It is designed as a complement to Global Navigation Satellite Systems (GNSS) so that a multi-system shipborne radionavigation receiver (IMO, 2015) can continuously support mariners with reliable positioning, navigation, and timing (PNT) data for their navigational duties. This is most impor-

tant in cases when GNSS is not available or shows reduced performance due to intentional or unintentional interference.

The system and service level parameter requirements of a navigation system, which is primarily used to assist the navigation of ships, are given by two resolutions of the International Maritime Organization (IMO; IMO, 2002, 2011). In the current stage of development, the R-Mode system is planned to be a secondary or backup system. For such a system, the user requirements with respect to horizontal position accuracy are given by the Recommendation R-129 of the International Association of Marine Aids to Navigation and Lighthouse Authorities (IALA) with 100 m for coastal navigation and 10 m for port approaches

This is an open access article under the terms of the [Creative Commons Attribution](https://creativecommons.org/licenses/by/4.0/) License, which permits use, distribution and reproduction in any medium, provided the original work is properly cited.

© 2021 The Authors. *NAVIGATION* published by Wiley Periodicals LLC on behalf of Institute of Navigation.

and navigation in restricted waters (IALA, 2012). As these numbers were derived from requirements for a future GNSS (IMO, 2002), it can be assumed that the numbers are related to a probability of 95% as it is defined for current worldwide radionavigation systems for the same operational areas (IMO, 2011).

The idea of R-Mode was born in the year 2008 with a proposal to use existing maritime infrastructure as a source for navigation information (Oltmann & Hoppe, 2008). This could be a cost-effective way to establish a navigation system beside GNSS for areas with high traffic density and challenging conditions. Three feasibility studies published in 2014, which were created as part of the ACCSEAS project, showed that R-Mode could work when medium frequency (MF) maritime radio beacons or base stations of the Automatic Identification System (AIS), operating in the very high frequency (VHF) band, are modified such that they broadcast synchronized R-Mode signals (Johnson & Swaszek, 2014a, 2014b, 2014c). These activities are continued today including the investigation of feasibility studies in different countries and the first R-Mode testbeds (Gewies et al., 2018; Grundhöfer & Gewies, 2020; Hoppe et al., 2018; Jiang et al., 2018; Johnson et al., 2020; Lee et al., 2018; Safar et al., 2019; Wirsing et al., 2020). The standardization of R-Mode has started (IALA, 2020).

This paper focuses on MF R-Mode as it was firstly outlined by Swaszek (2014), tested in the ACCSEAS project, as well as further developed and implemented within the project R-Mode Baltic (Gewies et al., 2018). Here, R-Mode is realized by adding two continuous wave signals next to the minimum-shift keying (MSK) modulated stream of code differential GNSS corrections of each station. As traditional marine beacons, the R-Mode beacons transmit the corrections in our testbed at a data rate of 100 bit/s in 500-Hz wide channels assigned to them by the IALA. Figure 1 shows the modified beacon signal of the transmitter site Rozewie which is part of the R-Mode testbed in the Southern Baltic Sea. Clearly visible is the modulated signal with the aiding carriers 225 Hz apart from the carrier frequency. Phase estimations of both carriers enables the determination of pseudoranges to the transmitter site (Swaszek, 2014) and that the positioning of at least three R-Mode signals are available (Johnson et al., 2017). Moreover, the first field trials have shown that MF R-Mode is capable of providing a positioning solution on land (Johnson et al., 2020).

This paper reports on MF R-Mode receiver developments and the first maritime test in the Southern Baltic Sea where seven radio beacons of the German Federal Waterways and Shipping Administration (WSV), Swedish Maritime Administration (SMA), and Maritime Office Gdynia (MOG) were equipped with R-Mode-ready signal

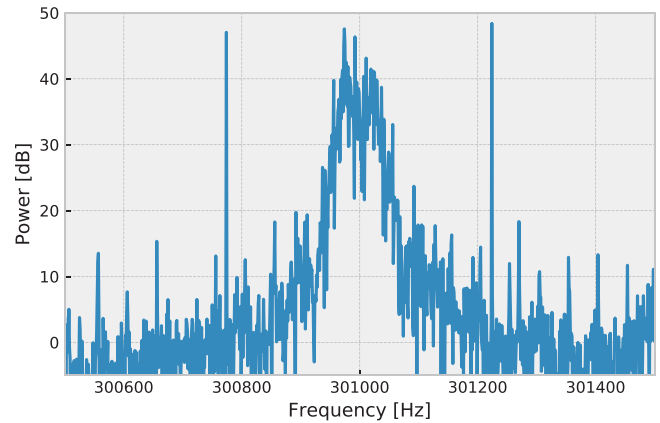


FIGURE 1 Measured spectrum of R-Mode signal from the station Rozewie [Color figure can be viewed in the online issue, which is available at wileyonlinelibrary.com and www.ion.org]

modulators (Gewies et al., 2018) that were synchronized to 10 ns accuracy by means of GNSS-stabilized atomic clocks that could easily be replaced by another timing source in the future. During our trials the R-Mode beacons did not transmit R-Mode navigation information. Therefore, estimation of time was not the target of this study.

The paper focuses on the description of the basic algorithm to obtain the phase and pseudorange estimates. Moreover, it shows how to obtain the position from the pseudorange measurements and compares the results of the first measurements with the accuracy bounds for coastal navigation and port approaches as requested by international organizations.

2 | PARAMETRIC ESTIMATION

In this section, we introduce two methods for estimating the phase of a continuous wave (CW). We need a signal model for this. For a single tone, this can be described as:

$$b_0 \sin(\omega_c t + \theta) \quad (1)$$

with the three parameters frequency ω_c , amplitude b_0 , and phase θ .

It is a major task in signal processing to deliver good estimation for this parameter. We consider the frequency as known. However the amplitude and especially the phase have to be estimated in the medium-frequency range. As we are interested in a discrete sampled signal, the time t can be quantized to t_n with constant sample rate t as:

$$t_n(n) = t_0 + n \frac{1}{f_{\text{sample}}} = (n_0 + n) \frac{1}{f_{\text{sample}}} \quad (2)$$

In this case, the bound can be given by:

$$\text{var}\{\hat{\theta}\} \geq \frac{\sigma^2}{b_0^2 N} \quad (3)$$

for a complex signal model (Rife & Boorstyn, 1974). Here $\hat{\theta}$ is the estimated phase parameter, σ^2 is the variance in the power density function (PDF) of the noise, and N is the total number of samples.

To obtain phase estimation, we suggest using a maximum likelihood estimation (Rife & Boorstyn, 1976). The likelihood function is given as:

$$L = \sum_{i=1}^k \{2b_i \text{Re}[e^{j\hat{\theta}_i} A(\omega_i)] - b_i^2\} \quad (4)$$

with:

$$A(\omega) = \frac{1}{N} \sum_{n=0}^{N-1} (X_n + jY_n) e^{-jn\omega_i \Delta t} \quad (5)$$

where X is defined as the input vector of samples and Y as the corresponding Hilbert transform. Both vectors have the length N and are indexed with n . k is the number of tones to estimate, with each tone defined according to our signal model (1), hereby i indicates the current frequency to evaluate within the sum. To find the parameters that maximize L , we need to maximize $A(\omega)$. Therefore, we obtain our estimates by:

$$\hat{b}_0 = |A(\omega_c)| \quad (6)$$

and:

$$\hat{\theta} = \arg[e^{-j\omega_c t_0} A(\omega_c)] \quad (7)$$

We assume that we know the frequency ω_c of the tone and obtain the estimates $\hat{\theta}$ for the phase and \hat{b}_0 for the amplitude. To estimate the range, we are interested in the phase estimates for different tones in parallel, so the presented approach does not scale very well and leads to relatively high computational effort.

However, it is widely known that a discrete Fourier transform (DFT) can be used for a parametric estimation (Kay, 1993; Rife & Boorstyn, 1976; Stoica et al., 1989), since we can describe $A(\omega)$ from (4) using the DFT base function:

$$e^{-j2\pi \frac{K}{N} n} \quad (8)$$

with:

$$\omega = 2\pi \frac{K f_{\text{sample}}}{N} \quad (9)$$

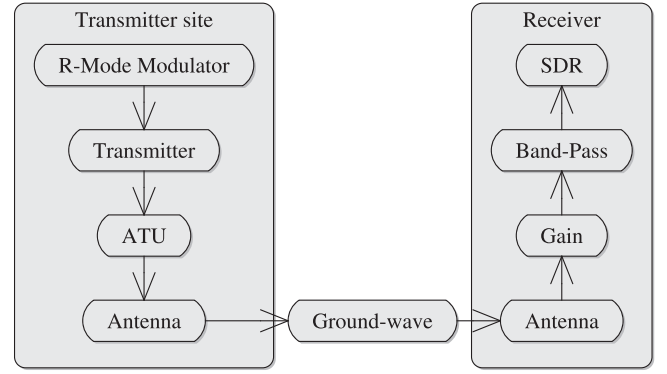


FIGURE 2 Block diagram of medium-frequency signal propagation

where K describes the point in the DFT spectrum. This yields to the matrix representation:

$$A(\omega) = \frac{1}{N} (X - jY)^T \begin{pmatrix} e^{-j0\Delta\omega t} \\ e^{-j1\Delta\omega t} \\ \dots \\ e^{-jN\Delta\omega t} \end{pmatrix} \quad (10)$$

which is one column of the transformation matrix of the DFT. With the fast Fourier transform (FFT), a computational-effective method is known to estimate N bins at once. The center frequencies of these bins are equally distributed at intervals of $\Delta\omega$ and need to match the continuous wave frequencies that we want to estimate. This otherwise leads to power leakages and reduced accuracy of the results. This is the main difference of the maximum likelihood estimate which can be calculated for any arbitrary frequency but is limited to one frequency per calculation.

Both estimation techniques result in complex numbers where the phase represents the needed phase information at the beginning of the observed time interval with length T . Therefore the positioning solution would generated with at least T s old data.

3 | SYSTEM BIAS AND PROPAGATION DELAY

After the signal has been generated at the transmitter site, it has to propagate to the receiver and pass different system components. Each of them will cause a delay or a distortion of the R-Mode signal.

Figure 2 shows the signal path as a generalized block diagram. The R-Mode signal is generated in a well-synchronized R-Mode modulator which provides the aiding carriers with a zero crossing (rising) at full seconds.

From the modulator, the signal is passed to the transmitter followed by the antenna tuning unit (ATU) and the antenna as the last part of the transmitter chain. It was shown that each of these elements cause a phase offset. The characterization of these effects is the subject of ongoing research (Grundhöfer et al., 2019; Grundhöfer & Gewies, 2020).

After transmission, the signal propagates as a ground-wave to the receiver where it is received by an antenna (see Figure 2). From there, it is passed to an active band-pass filter with adjustable gain and, finally, to the software-defined radio (SDR). As for the transmitter site, each of the components introduces a certain phase shift.

In addition, the signal propagates along a second path towards the ionosphere where it is attenuated significantly by the E-layer of the ionosphere at daytime. At night, this absorbing layer disappears and the signal is reflected at higher layers. This propagation path is called a *sky-wave*. At the receiver site, the ground-wave and sky-wave superimpose leading to a degenerate phase estimate at night (Johnson & Swaszek, 2014c). Currently, different mitigation techniques are under discussion to make the service available during the night (Grundhöfer et al., 2020). Solving this problem is beyond the scope of this paper.

In the following, it is assumed that all system components at the transmitter and receiver site are stable with respect to the introduced phase offsets. Summing over these offsets will result in a transmitter, receiver site, and aiding carrier-dependent system bias $\theta_{\text{system},i}$. The index i denotes in the following the aiding carrier i . The propagation causes a time delay $t_{p,i}$ of the carrier. Both effects together cause an accumulated phase delay at the receiver of $\theta_{\text{system},i} + \omega_i t_{p,i}$ for the carrier with angular frequency ω_i .

Due to the periodic nature of trigonometric functions, we have no access to the accumulated phase at the receiver site for the signal model in (1). The difference between the transmitted and received signal is θ_i is reduced by a number m_i of completed cycles 2π since transmission. This leads to ambiguities in the estimation of the range, which can be described in terms of the system bias and the propagation delay as:

$$\theta_i - m_i 2\pi = -(\theta_{\text{system},i} + \omega_i t_{p,i}) \quad (11)$$

Both, $t_{p,i}$ and m_i depend on the carrier and the distance to the transmitter.

The system bias of the transmitter sites in the R-Mode Baltic testbed is unknown. Therefore, this has to be estimated during a calibration step in the field. This step will also provide the number m_i . With $\theta_{\text{cal},i}$ as a calibration

parameter, we can deduce $t_{p,i}$ as:

$$t_{p,i} = \frac{\theta_{\text{cal},i} - \theta_i}{\omega_i} \quad (12)$$

with:

$$\theta_{\text{cal},i} = -\theta_{\text{system},i} + m_i 2\pi \quad (13)$$

This approach works well as long as the rover does not change position so much that θ_i reaches 0 or 2π . To prevent unrealistic jumps of $t_{p,i}$, the phase θ_i has to be tracked after fixing m_i so that it can grow above 2π or decrease below 0.

The pseudorange P_i between the rover and the transmitter site can be calculated using the phase velocity $c_{\text{ground},i}$ of the ground-wave with:

$$P_i = t_{p,i} c_{\text{ground},i} \quad (14)$$

However, as the R-Mode signal propagates as a ground-wave, the phase velocity depends on the frequency and conductivity of the ground (Guard, 1992; Wait, 1998). For propagation over sea water we assume a phase velocity of 299,616,913 m/s based on calculation done by GRWave (Rotherham, 1981). This value is valid for our test area, as we take the conductivity of the Baltic Sea as a reference. Due to a different ground conductivity of land, the phase velocity differs for a path over land.

If the propagation path is composed of different segments of land and sea paths then (14) is obviously wrong. But if we assume there is little or no change in the propagation speed over land, we can use (14) as an approximation and put the nearly constant error as an additional bias into the calibration system bias $\theta_{\text{system},i}$. Another bias occurs due to the movement of the vessel. As the estimation averages over time and the distance varies over time, our estimation has a velocity-dependent bias.

4 | LEAST SQUARES

As described in Section 3, the signal propagates as a ground-wave. Consequently, the geometrical distance between transmitter and receiver cannot be described as a line-of-sight distance (direct and straight line) which is given by the classical Euclidean distance formula. For the MF R-Mode system, the geometrical distance is given by the so-called *geodesic curve* or simply *geodesic* (Jekeli, 2016) which describes the minimum distance between two points on the Earth, assumed to be a perfect ellipsoid. The WGS84 is used as a reference system in order to localize the vessels on the sea. Given the non-linearity of the problem, a least squares (LS) adjustment algorithm that is used to

estimate the receiver position and clock bias as described in Groves (2008).

The system of equations contains three unknowns represented by the user geodetic latitude ϕ_u , the geodetic longitude λ_u , and the receiver clock bias δt with respect to the R-Mode system time. The pseudorange P that is obtained as an output from the phase tracker, which also considers the calibration bias, can be modeled as follows:

$$P_i = \rho_i + \delta t + \epsilon_i \quad (15)$$

where i represents the station index, ρ is the geometrical distance (geodesic), and ϵ is a noise term. The geodesic ρ can be computed by using Vincenty's approach which is based on an iterative algorithm (Vincenty, 1975). It also provides estimates for the forward and backward bearing angles that can be used to directly define the geometry matrix.

In general, for an over-determined system with m observations, the LS solution is (Groves, 2008; Subirana et al., 2013):

$$\mathbf{x}_l = \mathbf{x}_{l-1} + \mathbf{M}(\mathbf{H}^T \mathbf{W} \mathbf{H})^{-1} \mathbf{H}^T \mathbf{W} \mathbf{y}_{l-1} \quad (16)$$

where l is the algorithm recursion index. \mathbf{x}_l represents the update estimate $(\phi_{u_l}, \lambda_{u_l}, \delta t_l)^T$, whereas \mathbf{x}_{l-1} is the previous estimate $(\phi_{u_{l-1}}, \lambda_{u_{l-1}}, \delta t_{l-1})^T$ of the unknowns. \mathbf{H} is the geometry matrix and \mathbf{W} is a weighting matrix whereas $\mathbf{M} \in \mathbb{R}^{3 \times 3}$ represents a transformation matrix that can be obtained as follows (Groves, 2008):

$$\mathbf{M} = \begin{pmatrix} 1/R_M(\phi_{u_{l-1}}) & 0 & 0 \\ 0 & 1/[R_E(\phi_{u_{l-1}}) \cos \phi'_{l-1}] & 0 \\ 0 & 0 & 1 \end{pmatrix} \quad (17)$$

with $R_M(\phi)$ meridional or north-south curvature radius, $R_E(\phi)$ transverse or east-west curvature radius, and ϕ' angle subtended by an east-west great circle that subtends a unit longitude change. These values depend on the latitude of the user and are calculated as follows (Groves, 2008):

$$R_M(\phi) = \frac{a(1 - e^2)}{(1 - e^2 \sin^2 \phi)^{3/2}} \quad (18)$$

$$R_E(\phi) = \frac{a}{(1 - e^2 \sin^2 \phi)^{1/2}} \quad (19)$$

$$\cos \phi' = \sqrt{1 - \frac{R_M^2(\phi)}{R_E^2(\phi)}(1 - \cos^2 \phi)} \quad (20)$$

where a and e are the semi-major axis and eccentricity of the WGS84 ellipsoid.

In our approach, the geometry matrix $\mathbf{H} \in \mathbb{R}^{m \times 3}$ containing the unitary line-of-sight vector components in the navigation frame can be obtained exploiting the bearing angle α , provided by the Vincenty formula, as (RTCM Special Committee 127, 2016):

$$\mathbf{H} = \begin{pmatrix} \cos \alpha_1 & \sin \alpha_1 & 1 \\ \cos \alpha_2 & \sin \alpha_2 & 1 \\ \vdots & \vdots & \vdots \\ \cos \alpha_n & \sin \alpha_n & 1 \end{pmatrix} \quad (21)$$

In general, the weighting matrix $\mathbf{W} \in \mathbb{R}^{m \times m}$ takes into account the difference in the data quality (Subirana et al., 2013). Since the characterization of the measurements error has not been performed for the MF R-Mode transmitters, the weighting matrix is assumed to be a diagonal matrix where all the stations are treated equally (i.e., all values on the diagonal are set to 1). Last but not least, we define \mathbf{y}_{l-1} as pre-fit residuals obtained as follows:

$$\mathbf{y}_{l-1} = \begin{pmatrix} P_1 - \hat{\rho}_{1_{l-1}} \\ P_2 - \hat{\rho}_{2_{l-1}} \\ \vdots \\ P_n - \hat{\rho}_{n_{l-1}} \end{pmatrix} \quad (22)$$

where $\hat{\rho}_{i_{l-1}}$ represents the geodesic for the previous estimated point to i -th station.

The algorithm presented here was implemented in Python and integrated into the processing which is described in more detail in Section 5.2.

5 | TEST SETUP

5.1 | Hardware

The current setup for the R-Mode positioning test is comprised of two main components: an R-Mode receiver developed in the German Aerospace Center (DLR; Grundhöfer & Gewies, 2018), which is able to track all MF R-Mode signals of transmitters in the service area where it is currently located, and a Saab R5 GNSS receiver, which makes use of the Atlas correction service, Hemisphere, to achieve a position accuracy of 8 cm using a real-time kinematic (RTK) positioning approach. The R5 receiver worked during the trial in the position fixed mode such that it provided accurate positioning for the calibration of the R-Mode receiver and for the reference trajectory for later data analysis.

The current hardware evolution of the DLR R-Mode research receiver utilizes off-the-shelf components to create an easy-to-replicate receiver design. Figure 3 shows the

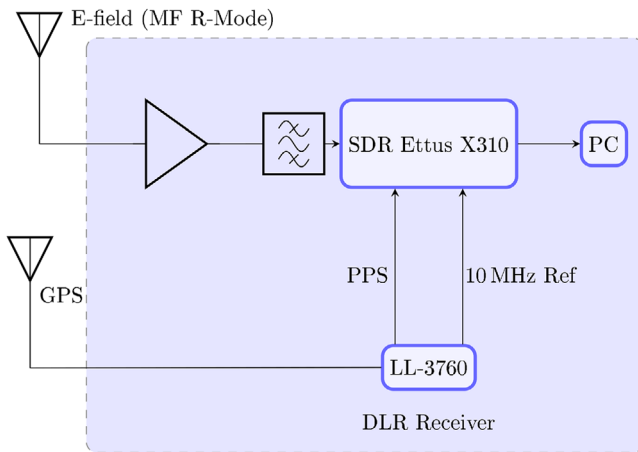


FIGURE 3 Block diagram of MF R-Mode receiver [Color figure can be viewed in the online issue, which is available at wileyonlinelibrary.com and www.ion.org]

wiring of the components as a block diagram. In the first stage, an active bandpass filter is used as an anti-aliasing filter, which also amplifies the signal by 30 dB. In our setup, we used a Krohn-Hite FBM3004 with a passband of between 285 kHz to 325 kHz.

The heart of the setup is built around the Ettus X310 SDR (Ettus Research, 2019) with a LFRX daughterboard. It is important to notice that this SDR is designed for differential-ended or quadrature-modulated signals.

The front end described here is single-ended with coax cable as interconnections. Therefore, each daughterboard supports up to two separated front ends, which can be used to compare different antennas. The sampled data of SDR will be processed at the computer as described in Section 5.2.

For performance tests of the R-Mode system, we utilized an external timing source, an LL-3760 GPS timing receiver from Lange-Electronic, that provides a pulse-per-second (PPS) and 10-MHz signal as a time reference to the SDR.

As an antenna, we use an E-field antenna called Boni-Whip, which is a short dipole with active matching to the desired frequency band.

5.2 | Software

The software for processing the obtained sample is organized into four main tasks. Figure 4 shows an overview of how each task interacts with the following one. Therefore, each routine has a name, an input interface, and an output interface, utilizing TCP sockets and ZeroMQ.

In the first step we have the SDR interface. This routine controls the SDR and its functionality. All the main settings for wiring the time source and antennas need to be defined

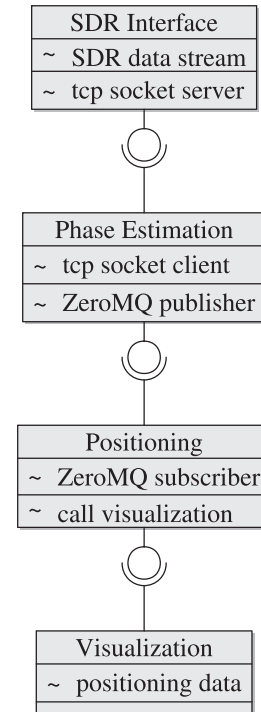


FIGURE 4 Block diagram of signal processing chain

here. Moreover, it is necessary to choose the desired channel and sample rate.

The interface hands over the samples to the right phase estimator. To simplify the processing, this routine creates chunks of samples for a period of 1 s. Each chunk is timestamped on the first sample. The size of the chunk is chosen according to the minimum observation time required in the receiver.

The chunks are handed via a TCP port into the phase estimation routine. Here, the phase is determined with a parametric estimation. To deliver a phase estimation near to real time, the execution time of any estimate is crucial. Therefore, we decided to implement the FFT as phase estimator on our current receiver design. According to Section 2, this corresponds to a maximum likelihood estimation with a bandwidth of 1 Hz for 1 s of observation time.

The cyclic nature of the R-Mode signal with its wavelength of about 1 km leads to jumps in the estimated phase after a few minutes of sailing. These jumps are then seen in the form of ambiguities in distance estimates. This complicates data processing when we want to reuse information from earlier epochs. Therefore, we implemented a phase tracking algorithm that compensates any phase jumps over the upper or lower phase limit of our estimator.

It adds multiples of 2π to the phase estimate so that the resulting phase never changes more than π from one epoch to the next. So the tracked phase starts between 0 and 2π

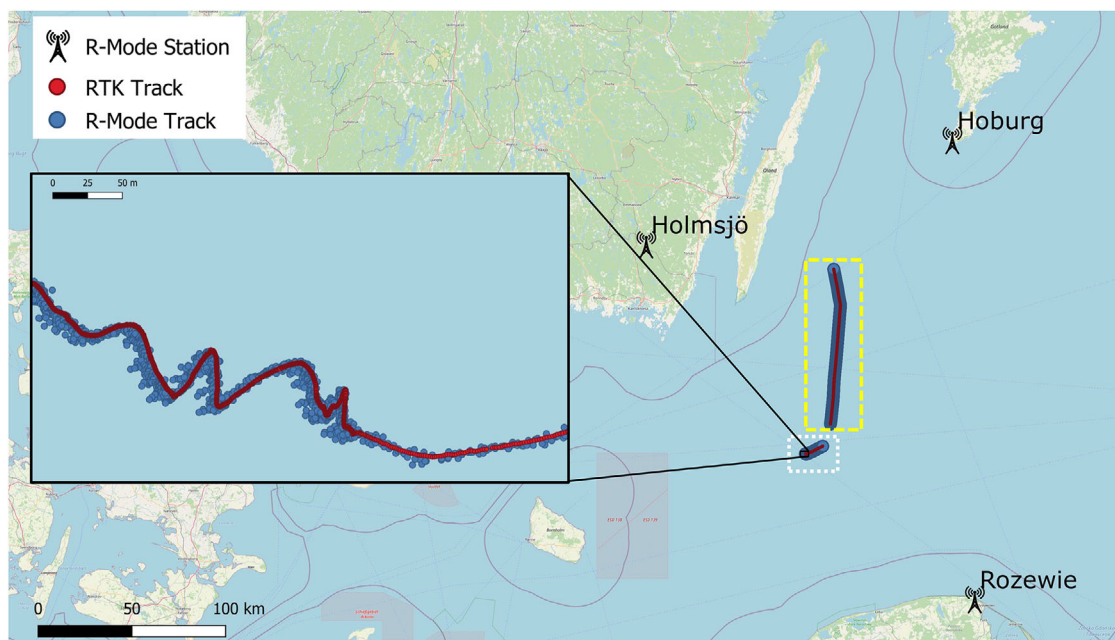


FIGURE 5 Track comparison between R-Mode and RTK (The map data was provided by OpenStreetMap©contributors [Online]) [Color figure can be viewed in the online issue, which is available at wileyonlinelibrary.com and www.ion.org]

but can reach very large values after hours of continuous signal tracking.

The tracked phase needs to be corrected for any bias described in Section 3. This bias is obtained during the calibration step. Here, the difference of the expected phase, which is calculated based on the known own position (e.g., from GNSS), and the measured phase is averaged over a defined time and taken as a bias. It is different for every station and every continuous wave component. For the R-Mode measurement on land, a similar approach was proposed (Johnson et al., 2020), but they assumed a fixed position. The obtained biases are used to correct all future estimations.

After the calibration, GNSS data are no longer required, as we expect that the bias is constant during our measurements. The speed of light for propagation over sea water is used to calculate a range, which is handed over in the next processing routine. This is done by using a publisher subscriber pattern from zeroMQ (Sústrík, 2020), as the execution time is crucial to prevent memory overflow and the ranges drastically reduce memory consumption. The pattern works as a buffer and enables distribution of the ranges to different positioning algorithms in the future.

The positioning routine implements the least squares algorithm presented in Section 4. The obtained position and clock error is saved with a timestamp in a comma-separated values (CSV) file and called a *first visualization*. This file can be read later on by the visualization routine to examine the data more closely and present it in an attractive way.

6 | RESULTS

In August 2020, we conducted a measurement campaign in the R-Mode Baltic testbed with the Fyrbyggaren, a buoy-tender vessel provided by the SMA. As described in Section 5, the DLR R-Mode receiver and the Saab R5 GNSS RTK receiver were set up on the ship. The DLR receiver was continuously tracking the signals of the MF R-Mode stations with the best signal quality while the Saab R5 receiver continuously provided a highly accurate ship position which was used for real-time calibration of the R-Mode receiver and as a reference for the performance estimation of R-Mode. Furthermore, the DLR receiver was able to perform R-Mode real-time positioning at sea. The results of two data sets, where the ship was sailing through the center of the testbed, are presented in this paper.

The track of the Fyrbyggaren for both data sets are shown in Figure 5 together with the R-Mode transmitter sites of the three strongest signals (Holmsjö, Hoburg, and Rozewie) in that region. The first data set is surrounded by a white rectangle and the second by a yellow rectangle. An inset shows in detail the deviation of the R-Mode-based track in blue from the RTK track in red. There is a gap between both data sets because we performed experiments with a different sampling rate over some hours.

During the measurements, the ship was sailing for several hours between the three transmitters, not far away from the center between them. The horizontal dilution of precision (HDOP) was better than 1.7 for all times which

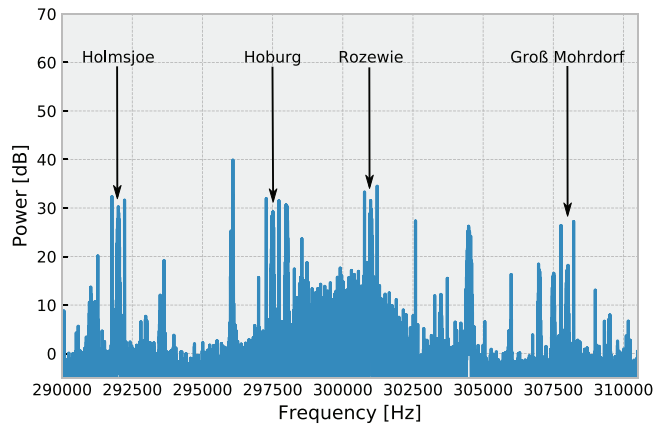


FIGURE 6 Overview of measured frequency spectrum at 5:50 UTC [Color figure can be viewed in the online issue, which is available at wileyonlinelibrary.com and www.ion.org]

is a good precondition to obtain accurate position estimations.

The first data set was logged for roughly 90 minutes in the morning, about 1.5 hours after sunrise, on August 31. Clearly visible in the inset of Figure 5, the R-Mode position follows the RTK position with some systematic scatter southwards as the ship was sailing at different speeds and the sea waves were small.

The second data set was logged on the same day for slightly less than five hours after noon. In contrast to the first data set, the ship sailed faster and had stronger waves from the direction we were sailing. Figure 5 shows that the propagation path of the signals from the Hoburg and Rozewie stations stayed most of the time over sea, whereas for the Holmsjö signal, some variations of the signal delay was expected because of the changing length of the land path component.

In both cases, the three transmitters of Holmsjö, Hoburg, and Rozewie were used for positioning with the LS approach. Groß Mohrdorf, a fourth station could also be received (see Figure 6), but due to the smaller signal-to-noise ratio (SNR) and the fact that we do not weight the stations in our current approach, the position became worse when including Groß Mohrdorf.

At the beginning of both data sets, an initialization over 30 s took place. For data set one, this was a quasi-static calibration and for data set two, a dynamic calibration (speed of about 10 kn superimposed with movement of the ship due to sea waves) to estimate the biases in the system of transmitter, receiver, and propagation path for each CW of all R-Mode transmitters in view. To reduce the impact of noisy phase estimations of one CW on the position, we always considered both CW per transmitter site in the position estimation. We performed positioning with six tracked signals of the three nearest R-Mode transmitters.

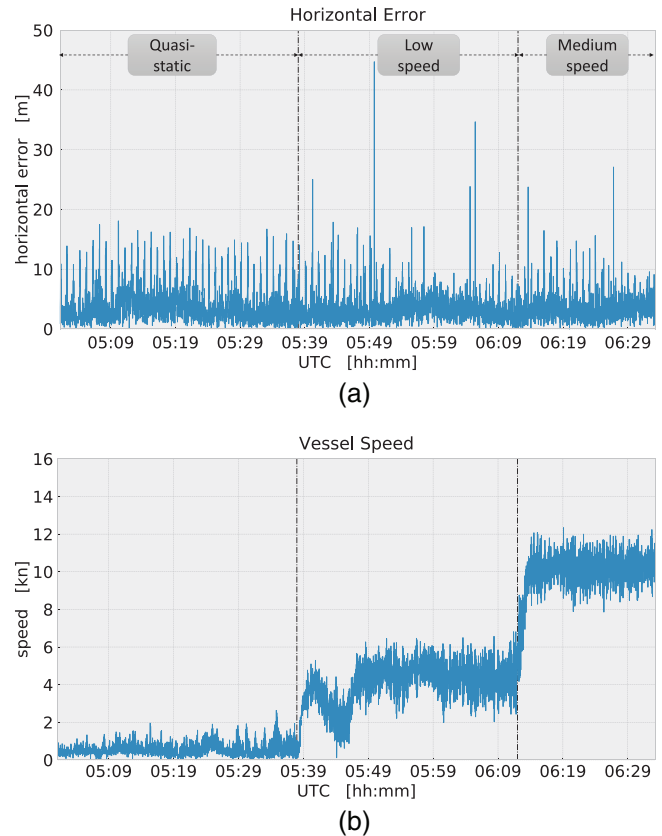


FIGURE 7 (a) Horizontal position error and (b) RTK-based speed of the ship over the time for the first data set [Color figure can be viewed in the online issue, which is available at wileyonlinelibrary.com and www.ion.org]

To evaluate the positioning performance of the R-Mode receiver, the horizontal distance between the R-Mode and the reference position was calculated and considered as horizontal error. Of particular relevance were the maximum (ϵ_M), mean ($\bar{\epsilon}$) and 95 % bound (ϵ_{95}) of the horizontal error which were used for performance assessment.

It is important to mention that the antennas of the R-Mode and GNSS receiver were mounted on a horizontal traverse at a distance of 25 cm on top of the ship's mast. This distance has been neglected in the initialization step and in the performance evaluation. Therefore, a horizontal error of up to 50 cm can be expected when the ship changes the heading after initialization.

6.1 | First data set

The first data set combines quasi-static and dynamic measurements. In particular, at the beginning of the data set, the ship was supposed to be in a static condition. However, some movements were caused by the presence of low wind speed and small waves. For this reason, this scenario is

referred to as *quasi-static*. The second part of the measurements was conducted with 5 kn speed, a scenario referred to as *low speed* whereas the last part was conducted with 10 kn speed and referred to as a *medium-speed* condition. The difference between the three aforementioned cases can be seen in Figure 7(b) that presents the speed of the ship obtained from the GNSS receiver.

Figure 7(a) shows the horizontal error of the R-Mode receiver over the entire data set. As expected, it coincides with the R-Mode and RTK track of Figure 5 where both are very close together. It appears that most of the epochs are characterized by an error significantly smaller than 10 m but the presence of repetitive spikes that overtake this value can be noted. A few outliers with more than 20 m are visible.

Figure 8 illustrates the *pseudorange error* (the difference between the R-Mode pseudorange and RTK-based calculated range) for the three used stations and for both CWs, designated as CW1 (low-frequency carrier) and CW2 (high-frequency carrier). The presence of fast variations which represent the noise on the pseudorange residual can be noted for the three stations. This is significantly smaller than 10 m most of the time.

On top of the noise, a small time-varying bias can be observed for all stations, which is most likely caused by the changes in the signal propagation path over land, which has so far not been modeled in the receiver (see Section 3). This assumption is justified because the bias on time scales of several minutes is correlated for the CWs of one station. This is expected because changes in the propagation path affect both signals very similarly due to their nearly identical frequencies. On the other hand, the biases are different among different stations due to the fact that the signals travel along different paths and therefore are affected by distinct effects.

The pseudorange error for Holmsjö in Figure 8(a) provides the explanation for the spikes in the position error in Figure 7(a). It shows the same pattern. Every minute, the pseudorange error of both CWs increases for 7 s by 10 m to 15 m. Unfortunately, an explanation for this issue has not been found.

The 95% bound for the positioning error (ϵ_{95}) was mainly driven by the spikes of the Holmsjö pseudorange error. This caused a significant error in about 12% of the epochs and was independent of the speed of the vessel. ϵ_{95} is very similar for the three phases of quasi-static, low speed, and high speed with 10.3 m, 7.5 m, and 7.6 m, respectively.

The decrease of ϵ_{95} for the dynamic phases can be explained with a decrease of the Holmsjö pseudorange error (see Figure 8) caused by the superposition of the spikes and a negative bias for the time after 5:39 UTC (see Figure 8), which was caused by changes in the propagation path over land. For the entire data set, ϵ_{95} is 8.4 m, which is

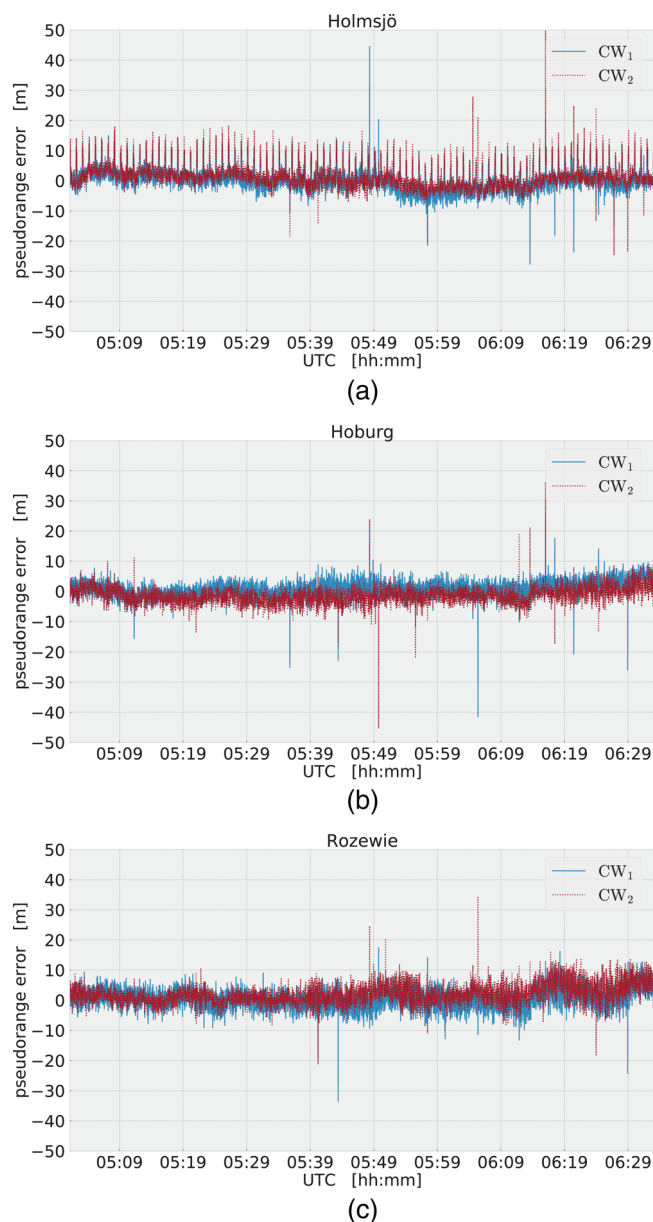


FIGURE 8 Pseudorange residuals of the first data set for (a) Holmsjö, (b) Hoburg, and (c) Rozewie [Color figure can be viewed in the online issue, which is available at wileyonlinelibrary.com and www.ion.org]

better than the requirement for navigation support of port approaches. Fixing the Holmsjö issue should considerably improve the performance.

The mean error $\bar{\epsilon}$ is a better measure for the R-Mode performance in this case, because it is not only affected by the Holmsjö issue. It reflects more than the noise of the pseudorange estimations. With 3.9 m, 3.4 m, and 3.5 m for the quasi-static, low-speed, and high-speed phases, and a value of 3.7 m for the entire data set, it is considerably lower than ϵ_{95} .

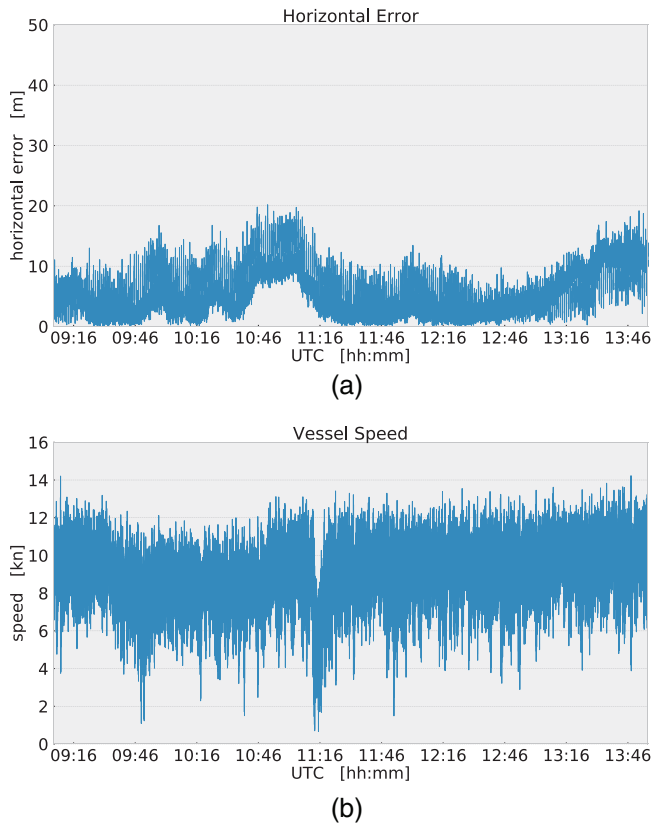


FIGURE 9 (a) Horizontal position error and (b) RTK-based speed of the ship over the time for the second data set [Color figure can be viewed in the online issue, which is available at wileyonlinelibrary.com and www.ion.org]

The maximum error ϵ_M reflects the outliers in the R-Mode positioning. It is 18.1 m for the quasi-static, 44.7 m for the low speed, and 27.1 m for the medium-speed phase of the experiment. The outliers are caused by jumps in the phase of the CW for a single station [see Figure 7(a) and Figure 8]. Such errors might be suppressed when pseudoranges with unrealistically large jumps are excluded from positioning.

6.2 | Second Data set

The second data set refers to a purely dynamic test in which the vessel was traveling with a speed of 10 kn and was experiencing adverse weather conditions with strong waves. This is visible in Figure 9(b), which shows the speed of the vessel obtained with the GNSS receiver. A higher variance of measurement, induced by the heavy sea-waves, can be observed when compared with Figure 7(b) where the same scale is adopted.

Figure 9(a) illustrates the R-Mode horizontal position error. An error smaller than 20 m characterizes most of the epochs and the presence of the repetitive spikes can also be

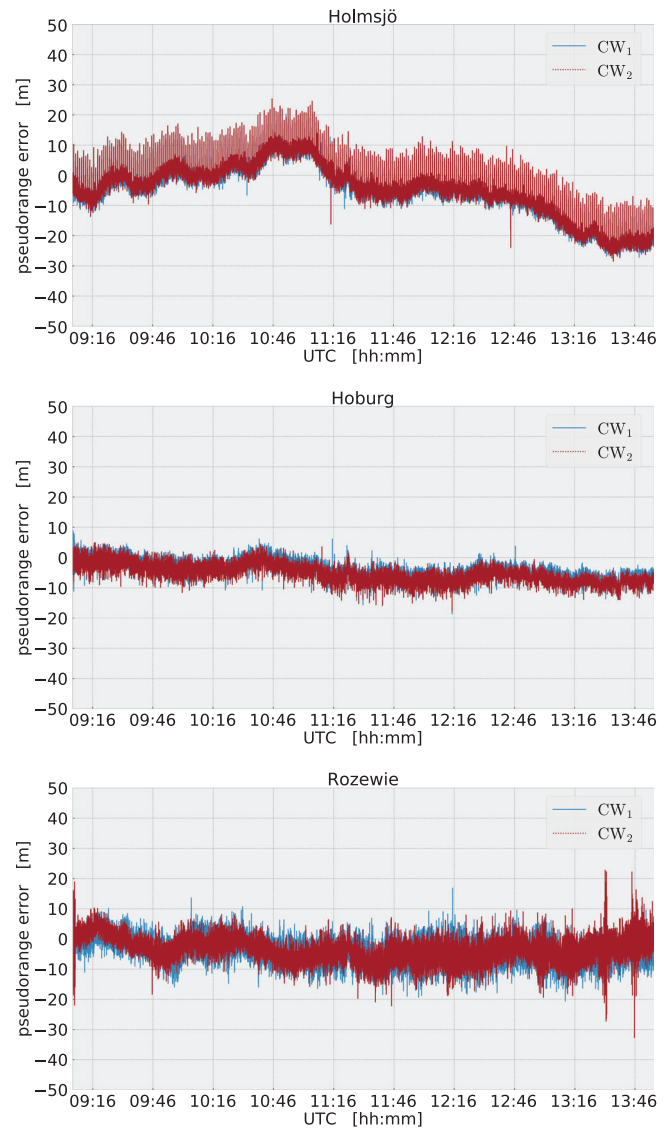


FIGURE 10 Pseudorange residuals of the second data set for (a) Holmsjö, (b) Hoburg, and (c) Rozewie [Color figure can be viewed in the online issue, which is available at wileyonlinelibrary.com and www.ion.org]

observed in this case. Compared to 7(a), a time-varying bias can be noted which causes a larger error from 10:20 to 11:15 and from 13:00 up until the end of the experiment. This strong bias is mainly induced by Holmsjö, as we see later.

Similarly to the first data set, Figure 10 presents the pseudorange residuals for the CWs of the transmitters. Hoburg [see 10(b)] was very stable during the measurements with a final small negative bias of approximately 5 m. Rozewie [depicted in Figure 10(c)] was also very stable but the noise level was slightly higher compared to Hoburg. As explained previously, the stability of these two stations comes from the fact that the signal traveled mostly over the sea.

TABLE 1 Horizontal error performance evaluated for the two data sets

Data	$\bar{\epsilon}$ [m]	ϵ_{95} [m]	ϵ_M [m]
Set 1 (Q-Static)	3.9	10.3	18.1
Set 1 (Low)	3.4	7.5	44.7
Set 1 (Medium)	3.5	7.6	27.1
Set 2	5.2	12.0	20.2

On the contrary, for Holmsjö [Figure 10(a)], the bias was strongly influenced by the land path component which was fluctuating severely during the movement of the vessel and induced an offset increase from 9:00 to 11:00 UTC and a decrease from 11:00 to 13:30 UTC. The repetitive spikes are clearly visible.

The 95% horizontal error was driven primarily by the spikes, as explained in Section 6.1. In this experiment ϵ_{95} was 12.0 m, which is slightly higher than the first data set value, but it is mainly due to the effect of the bias caused by Holmsjö. For the same reason, the mean horizontal error $\bar{\epsilon}$ was—at 5.2 m—also larger. These results were expected due to the larger variation in the ship's position during the 5 h time period and the uncompensated effect of the ground conductivity changes.

The maximum horizontal error ϵ_M , which can represent outliers, was 20.2 m. Compared to the first data set, jumps were not visible for all transmitters (see Figure 10) and therefore no considerable outliers could be identified.

6.3 | Performance Summary

The results of the performance obtained in the daytime measurement campaign in the center of the testbed are summarized in Table 1. In general, the difference between the two data sets, which deviates in the averaged speed of the ship and the additional movement due to waves, is only small. With an average horizontal position error of 5.2 m and a 95% error of 12.0 m, it is highest for the longest data set where the ship's movement was also most dynamic. The reason for the higher error is most likely due to the lack of compensation for the change in the land propagation path for the Holmsjö signal.

The maximum position error was obtained with 44.7 m as an outlier. Several outliers were recognized which have no significant impact on the 95% error because they are so rare. The technical issue at the Holmsjö transmitter did, however, cause an increase in the position error in 12% of the epochs.

We expect that the R-Mode positioning performance can be significantly improved when the technical issue of the Holmsjö transmitter is solved. Furthermore, applying compensation techniques for changes in the

propagation delays caused by changes of the ground conductivity between transmitter and receiver (ground conductivity) would decrease the position error. Such an approach is known from the eLoran system (Hargreaves et al., 2012).

The two analyzed experiments show that MF R-Mode has the potential to serve the mariner with position information suitable for coastal navigation. Even the 10 m limit for port approaches and navigation in restricted waters requested in the IALA Recommendation R-129 (IALA, 2012) appears to be reachable.

Please note, this study does not claim to fully represent the MF R-Mode performance under difficult conditions. It does not cover sky-wave-induced fading during the night and stronger variation of the land-sea path. The geometry was always good (see Figure 5).

7 | CONCLUSION

R-Mode is a navigation system under development. It consists of land-based infrastructure, as it was deployed in the R-Mode Baltic testbed, and an R-Mode receiver as a ship-site component, which is described here together with the results of the first sea trials in the testbed.

The paper gives an overview of the R-Mode receiver implementation of the German Aerospace Center. It shows in detail the implemented estimation theory for the phase of the continuous wave signal components based on an FFT approach, which enables an efficient track of an unlimited number of R-Mode signals in real-time. Furthermore, it introduces our approach for real-time calibration of the receiver under dynamic conditions and a 2-dimensional real-time single-point positioning approach which considers the ground-wave propagation of the R-Mode signal.

With the introduction of the R-Mode receiver, it has become possible to perform MF R-Mode-based positioning at sea for the first time. Under good conditions, we achieved a 95% real-time position accuracy of 12.0 m. This is in line with the requirements for a navigational backup system for a coastal area and nearly meets the requirement for port approaches and restricted waters as defined by IALA.

A detailed analysis of the pseudoranges showed that technical problems at one station and uncompensated signal delays caused by changes of ground conductivity over time are major sources of error in the measurements. Mitigation of both effects should increase the performance.


Our future work will require a better characterization of the error sources presented in this paper, including system bias, sky-wave interference, and propagation path. Moreover, we want to use the phase difference to solve the

ambiguities in the pseudorange due to the cyclic nature of R-Mode signals.


ACKNOWLEDGEMENTS

The research was conducted in the framework of the R-Mode Baltic project that aims to set up the first combined medium frequency and very high frequency R-Mode testbed in the Southern Baltic Sea and show that R-Mode fulfills the maritime user requirements. The authors thank the entire R-Mode Baltic project team and especially our partners Saab AB (publ) TransponderTech, Gutek AB, and German Federal Maritime and Hydrographic Agency for their support in preparation and conduction of the sea trials. Furthermore, the authors thank the European Union for co-financing the R-Mode Baltic project through the European Regional Development Fund within the Interreg Baltic Sea Region Programme.

ORCID

Lars Grundhöfer  <https://orcid.org/0000-0002-8650-8280>

Stefan Gewies  <https://orcid.org/0000-0001-5549-8115>

Giovanni Del Galdo  <https://orcid.org/0000-0002-7195-4253>

REFERENCES

- Ettus Research (2019). X300 and X310 X Series [datasheet].
- Gewies, S., Dammann, A., Ziebold, R., Bäckstedt, J., Bronk, K., Wereszko, B., Rieck, C., Gustafson P., Eliassen C. G., & Hoppe, M. (2018). R-Mode testbed in the Baltic sea. *19th IALA Conference 2018*, Incheon, Republic of Korea. <https://elib.dlr.de/120702/>
- Groves, P. D. (2008). *Principles of GNSS, inertial, and multisensor integrated navigation systems*. Artech House.
- Grundhöfer, L., & Gewies, S. (2018). R-Mode receiver development for medium frequency signals. *Scientific Journals of the Maritime University of Szczecin*, 56, 57–62. <https://doi.org/10.17402/314>
- Grundhöfer, L. & Gewies, S. (2020). Equivalent circuit for phase delay in a medium frequency antenna. *2020 European Navigation Conference (ENC)*, Dresden, Germany. <https://doi.org/10.23919/ENC48637.2020.9317493>
- Grundhöfer, L., Gewies, S., Hehenkamp, N., Hoppe, M. & Walterfang, M. (2019). Characterization of a transmitter in a medium frequency maritime terrestrial navigation system. *2019 IEEE Intelligent Transportation Systems Conference (ITSC)*, Auckland, New Zealand, 3828–3832. <https://doi.org/10.1109/ITSC.2019.8916992>
- Grundhöfer, L., Gewies, S., Hehenkamp, N. & Del Galdo, G. (2020). Redesign waveforms in the maritime medium frequency bands. *2020 IEEE/ION Position, Location and Navigation Symposium (PLANS)*, Portland, OR, 827–831. <https://doi.org/10.1109/PLANS46316.2020.9110174>
- Guard, U. C. (1992). *Loran-C user handbook (Commandant Publication No. P16562.6)*. Washington, DC. <https://www.navcen.uscg.gov/?pageName=loranHandBook>
- Hargreaves, C., Williams, P. & Bransby, M. (2012). ASF quality assurance for eLoran. *Proc. of the 2012 IEEE/ION Position, Location and Navigation Symposium*, Myrtle Beach, SC, 1169–1174. <https://doi.org/10.1109/PLANS.2012.6236972>
- Hoppe, M., Grant, A., Hargreaves, C. & Williams, P. (2018). R-Mode: The story so far. *Proc. of the 19th IALA Conference 2018*, Incheon, Republic of Korea.
- International Association of Lighthouse Authorities (2012). *R0129 GNSS vulnerability and mitigation measures* (Technical Report No. R-129). <https://www.iala-aism.org/product/gnss-vulnerability-and-mitigation-measures-r-129/>
- International Association of Lighthouse Authorities (2020). *VDES R-Mode* (Guideline No. G1158). <https://www.iala-aism.org/product/g1158-vdes-r-mode/>
- International Maritime Organization (2002). Resolution A.915(22) Revised maritime policy and requirements for a future GNSS (Technical Report). [https://wwwcdn.imo.org/localresources/en/KnowledgeCentre/IndexofIMOResolutions/AssemblyDocuments/A.915\(22\).pdf](https://wwwcdn.imo.org/localresources/en/KnowledgeCentre/IndexofIMOResolutions/AssemblyDocuments/A.915(22).pdf)
- International Maritime Organization (2011). *Resolution A.1046(27): Worldwide radionavigation system* (Technical Report). [https://wwwcdn.imo.org/localresources/en/KnowledgeCentre/IndexofIMOResolutions/AssemblyDocuments/A.1046\(27\).pdf](https://wwwcdn.imo.org/localresources/en/KnowledgeCentre/IndexofIMOResolutions/AssemblyDocuments/A.1046(27).pdf)
- International Maritime Organization (2015). Resolution MSC.401(95): Performance standards for multi-system shipborne radionavigation receivers (Technical Report). [https://wwwcdn.imo.org/localresources/en/KnowledgeCentre/IndexofIMOResolutions/MSCResolutions/MS.401\(95\).pdf](https://wwwcdn.imo.org/localresources/en/KnowledgeCentre/IndexofIMOResolutions/MSCResolutions/MS.401(95).pdf)
- Jekeli, C. (2016). *Geometric reference systems in geodesy*. Ohio State University. <http://hdl.handle.net/1811/77986>
- Jiang, Y., Wu, J., & Zhang, S. (2018). An improved positioning method for two base stations in AIS. *Sensors*, 18, 4(4):<https://www.mdpi.com/1424-8220/18/4/991>. <https://doi.org/10.3390/s18040991>
- Johnson, G., Dykstra, K., Ordell, S. & Swaszek, P. (2020). R-mode positioning system demonstration. *Proc. of the 33rd International Technical Meeting of the Satellite Division of the Institute of Navigation (ION GNSS+ 2020)*. <https://doi.org/10.33012/2020.17728>
- Johnson, G., & Swaszek, P. (2014a). *Feasibility study of R-Mode combining MF DGNSS, AIS, and eLoran transmissions* (Technical Report). ACCSEAS. https://www.iala-aism.org/content/uploads/2016/08/accseas_r_mode_feasibility_study_combined_dgnss_ais_and_eloran.pdf
- Johnson, G., & Swaszek, P. (2014b). *Feasibility study of R-mode using AIS transmissions: Investigation of possible methods to implement a precise GNSS independent timing signal for AIS transmissions* (Technical Report). ACCSEAS.
- Johnson, G., & Swaszek, P. (2014c). *Feasibility study of R-mode using MF DGPS transmissions* (Technical Report). ACCSEAS. https://www.iala-aism.org/content/uploads/2016/08/accseas_r_mode_feasibility_study_mf_dgps_transmissions.pdf
- Johnson, G., Swaszek, P., Hoppe, M., Grant, A. & Safar, J. (2017). Initial results of MF-DGNSS R-Mode as an alternative position navigation and timing service. *Proc. of the 2017 International Technical Meeting of the Institute of Navigation*, Monterey, CA, 1206–1226. <https://doi.org/10.33012/2017.14886>
- Kay, S. M. (1993). *Fundamentals of statistical signal processing: Estimation theory, volume 1*. Prentice-Hall, Inc.
- Koch, P., & Gewies, S. (2020, Mar). Worldwide availability of maritime medium-frequency radio infrastructure for R-Mode-supported navigation. *Journal of Marine Science and Engineering*, 8(3), 209. <https://doi.org/10.3390/jmse8030209>
- Lee, S., Han, Y., Park, S. H., Seo, K. & Fang, T. H. (2018). Feasibility analysis of R-Mode in R.O.K. from MF beacon station deployment. *19th IALA Conference 2018*.

- Oltmann, J. H. & Hoppe, M. (2008). *Contribution to the IALA world-wide radio navigation plan (IALAWWRNP) / recapitalization of MF DGNSS systems* (Input document to IALA ENAV4).
- Rife, D. C., & Boorstyn, R. (1974). Single tone parameter estimation from discrete-time observations. *IEEE Transactions on Information Theory*, 20(5), 591–598. <https://doi.org/10.1109/TIT.1974.1055282>
- Rife, D. C., & Boorstyn, R. R. (1976). Multiple tone parameter estimation from discrete-time observations. *The Bell System Technical Journal*, 55(9), 1389–1410. <https://doi.org/10.1002/j.1538-7305.1976.tb02941.x>
- Rotherham, S. (1981). Ground-wave propagation. Part 1: Theory for short distances. *IEE Proc. for Communications, Radar, and Signal Processing*, 128(5), 275–284. <https://digital-library.theiet.org/content/journals/10.1049/ip-f-1.1981.0046>
- Radio Technical Commission for Maritime Services Special Committee 127. (2016). *Minimum performance standards for marine eLoran receiving equipment* (Technical Report No. RTCM 12700.0).
- Safar, J., Grant, A., Williams, P., & Ward, N. (2019). Performance bounds for VDES R-Mode. *Journal of Navigation*, 73(1), 92–114. <https://doi.org/10.1017/S0373463319000559>
- Stoica, P., Moses, R. L., Friedlander, B., & Soderstrom, T. (1989). Maximum likelihood estimation of the parameters of multiple sinusoids from noisy measurements. *IEEE Transactions on Acoustics, Speech, and Signal Processing*, 37(3), 378–392. <https://doi.org/10.1109/29.21705>
- Subirana, S. J., Juan Zornoza, J. M., & Hernández-Pajares, M. (2013). *GNSS data processing, volume I: Fundamentals and algorithms*. European Space Agency Communications.
- Swaszek, P. F., Johnson G. W., Alberding J., Hoppe M. & Oltmann J.-H. (2014). Analysis of MF-DGNSS modifications for improved ranging. *European Navigation Conference (ENC) 2014*, Rotterdam, Netherlands.
- Sústriak, M. (2020). *The architecture of open source applications, volume II: Structure, scale, and a few more fearless hacks*. ZeroMQ. <http://www.aosabook.org/en/zeromq.html>
- Vincenty, T. (1975). Direct and inverse solutions of the geodesics on the ellipsoid with application of nested equations. *Survey Review*, 23(176), 88–93.
- Wait, J. R. (1998). The ancient and modern history of EM ground-wave propagation. *IEEE Antennas and Propagation Magazine*, 40(5), 7–24. <https://doi.org/10.1109/74.735961>
- Wirsing, M., Dammann, A. & Raulefs, R. (2020). Designing a ranging signal for use with VDE R-Mode. *2020 IEEE/ION Position, Location and Navigation Symposium (PLANS)*, Portland, OR, 822–826. <https://doi.org/10.1109/PLANS46316.2020.9109855>

How to cite this article: Grundhöfer L, Rizzi FG, Gewies S, et al. Positioning with medium frequency R-Mode. *NAVIGATION*. 2021;68:829–841. <https://doi.org/10.1002/navi.450>